EARTH SURFACE PROCESSES AND LANDFORMS
Earth Surf. Process. Landforms **36,** 839–852 (2011)

Published online 9 December 2010 in Wiley Online Library
(wileyonlinelibrary.com) DOI: 10.1002/esp.2112

New challenges for tafoni research. A new approach to understand processes and weathering rates

M. Brandmeier,[1,2]* J. Kuhlemann,[1,3] I. Krumrei,[1] A. Kappler[1] and P.W. Kubik[4]
[1] Institute for Geosciences, University of Tübingen, Sigwartstr. 10, D-72076 Tübingen, Germany
[2] GZG, Institute for Geochemistry, University of Göttingen, Goldschmidt Str. 1, D-37077 Göttingen, Germany
[3] Swiss Federal Nuclear Safety Inspectorate CH-5232 Villigen-ENSI, Switzerland
[4] Laboratory of Ion Beam Physics, ETH Zurich, Schafmattstrasse 20, CH-8093 Zurich, Switzerland

Received 8 July 2009; Revised 19 October 2010; Accepted 28 October 2010

*Correspondence to: M. Brandmeier, GZG, Institute for Geochemistry, University of Göttingen, Goldschmidt Str. 1, D-37077. E-mail: mbrandm@gwdg.de

ESPL
Earth Surface Processes and Landforms

ABSTRACT: Cavernous tafoni-type weathering is a common and conspicuous global feature, creating artistic sculptures, which may be relevant for geochemical budgets. Weathering processes and rates are still a matter of discussion. Field evidence in the type locality Corsica revealed no trend of size variability from the coast to subalpine elevations and the aspect of tafoni seems to be governed primarily by the directions of local fault systems and cleavage, and only subordinately by wind directions or the aspect of insulation. REM analysis of fresh tafone chips confirmed mechanical weathering by the crystallization of salts, as conchoidal fracturing of quartz is observed. The salts are only subordinately provided by sea spray, as calcium and sodium sulfates rather than halite dominate even close to the coast. Characteristic element ratios compare well with aerosols from mixed African and European air masses. Sulfates are largely derived from Sahara dust, indicated by their sulfur isotopic composition. Salt crystals form by capillary rise within the rock and subsequent crystallization in micro-cracks and at grain boundaries inside rain-protected overhangs. Siderophile bacteria identified by raster electron microscopy (REM) analysis of tafone debris contribute to accelerated weathering of biotite and tiny sulfide ore minerals. By applying ^{10}Be-exposure dating, weathering rates of large mature tafone structures were found to be about an order of magnitude higher than those on the exposed top of the affected granite blocks.

KEYWORDS: tafoni; Corsica; cavernous weathering; weathering rates; salt weathering; ^{10}Be dating

Introduction

Weathering rates and processes play an important role in global chemical budgets in Earth system science, but cavernous weathering of crystalline rocks is considered a curiosity, despite its global distribution. The individual shapes of these sculptures, often forming human and animal faces, represent natural art. Cavernous, so-called tafone weathering was studied in the type locality Corsica. Tafoni (singular: tafone) typically have arched-shaped entrances, concave inner walls, overhanging visors and gently sloping debris-covered floors (Turkington and Phillips, 2004), but the term is not strictly defined in the literature.

In order to propose a model of tafone weathering that considers not only processes but also time-scales and the nature of the salts involved, geomorphological, geochemical and micromorphological data were integrated. The formation of tafoni is complex and may involve a combination of different processes operating on different parts of the landform (Mellor *et al*., 1997). It has been debated for many years and therefore we first present a short review of past and ongoing research.

Review of Historical Research on Tafone Weathering

The first reference to tafoni is found in a journey description by Tuckett (Tuckett, 1884) of his trip to Corsica in 1882. A report containing a draft was published 8 years later by Compton (Compton, 1892). Research on tafone weathering in the type locality reaches back more than 100 years. Early attempts to explain these weathering forms range from aeolian erosion to abrasion by snow in polar regions (Blackwelder, 1990). In ethnological science the origin of tafoni in coastal regions of California was attributed to the action of drilling-snails, as noted by Norwick and Dexter (2002). This interpretation was soon revised and chemical weathering was accepted as a major process in tafoni-type weathering (Dragovic, 1969; Twidale, 1976).

Worldwide occurrences of tafoni, including Australia (Bradley *et al*., 1978), the Mediterranean (Mustoe, 1983; Mellor, 1986; Mellor *et al*., 1997; Sancho and Benito, 1990), in the Midwest of the USA, the Sahara (Smith, 1978), the Namib desert (Ollier, 1978), Antarctica (Guglielmin *et al*.,

2005) and many coastal regions (Kelletat, 1980; Matsukura and Matsuoka, 1991; Mottershead and Pye, 1994; Hejl, 2005) have led to a general agreement that an arid period during the year is essential for the formation of tafoni. While it is largely accepted that lithology, the presence of salts, climate and exposition form a complex system of weathering conditions, the major processes controlling tafoni-type-weathering are poorly understood (Huinink *et al.*, 2004). The scientific approaches toward a better understanding vary from experimental work or computer-based simulations to idiographic studies with some quantitative analytics.

Traditionally, cavernous weathering has been seen as a diagnostic feature for arid and salt-rich regions, and salt weathering is generally accepted as the main process in the formation of tafoni. Crystals of salt on the walls of coastal and desert tafoni (McGreevy, 1985; Matsukura and Matsuoka, 1991; Mellor *et al*., 1997) and salt in debris particles of tafoni in Antarctica (Wellman and Wilson, 1965) support this theory. Salt increases the solubility of silicates, effective during wet periods, whereas mechanical weathering by crystallization of salts in fractures during dry periods is the main process in tafoni formation (Mustoe, 1982; Young, 1987). There is some debate as to whether the formation of crusts on the exposed surface or core-softening are of greater importance for cavernous weathering (Wilhelmy, 1964; Conca and Rossman, 1982; Robinson and Williams, 1987). Examples of tafoni without external crusts indicate that these are not critical for their genesis (Young, 1987; Kejonen and Lahti, 1988).

Recent publications have led to better understanding of the processes involved (Goudie and Viles, 1995). Processes of self-organization in an unstable, dynamic weathering system are proposed by Turkington and Phillips (2004). Huinink *et al*. (2004) show a computer-based model for the continous development of a small hole in a rock surface during several wetting–drying cycles by salt crystallization. McBride and Picard (2004) introduce a morphogenetic classification of tafoni and the formation of Turing-type diffusion cells based on processes of self-organization of salty pore waters.

There is a major deficiency concerning weathering rates and the origin of the constituents of the salts. Three publications propose equations for the temporal development of weathering rates of tafoni of known maximum ages (Matsukura and Matsuoka, 1991; Sunamura, 1996; Norwick and Dexter, 2002). The indirect age determination is based on the uplift of coastal platforms (Matsukura and Matsuoka, 1991) which does not necessarily coincide with the beginning of tafone evolution. These data, however, indicate that during the initial phase of tafoni formation and other cavernous weathering types, much higher rates occur than during the mature phase. This is best expressed by a geometry-related parabolic function, depending on various factors such as lithology and local climate setting.

Sampling Sites

The criteria for sampling locations were variations in the distance to the sea, geographic orientation, and altitude above sea level in order to evaluate the influence of sea spray and sea salts on weathering rates as well as climatic differences due to altitude and aspect. Sampling sites are restricted to granitoid rocks of Variscan age, since such rocks are most common and a potential impact of lithological differences on tafone weathering is reduced. As shown in Figure 1, Calvi, Île Rousse, Calanche and Eremitage de la Trinité represent coastal sites with altitudes of 150 m to 900 m above sea level. As inland sites we selected Bavella, Capu Aleri and the Cuscione plateau with altitudes of 1300 m to 1700 m above sea level, and the Bavella valley at 500 m above sea level.

Climatic conditions are an important factor in weathering. Corsica lies within the Mediterranean climate zone characterized by rainfall during winter and aridity during summer season when the Mediterranean lies within the subtropical high (Endlicher, 2000). In winter, cyclones influenced by the west-wind-zone bring heavy rainfalls from the west whereas temperatures may stay relatively mild in low regions and fair weather may occur due to a strong high (Azores). Average rainfall in Calvi varies between 364 mm and 862 mm while inland stations (Ghisoni) recorded amounts up to 2367 mm (Bruno and Giorgetti, 2001). It must also be considered that relief has a strong influence on local climate conditions. The prevailing winds (Libecciu, Grecale, Tramuntana, and Mistral) and their velocities are depicted in Figure 1.

Temperature distribution on an island depends on relief and distance to the sea. On coastal sites the yearly amplitude is much smaller than inland and temperature maxima reach 21–23°C and 10–12°C while minima range from 12 to 14°C and 6 to 8°C, respectively.

Analytical Methods

We subdivided our methodology into three different approaches. During fieldwork we collected geomorphological data (aspect, lichen growth, temperature, relative humidity variations, form, and vertical and horizontal dimensions of the tafoni). With this information for 61 tafoni we built a matrix which was then analysed statistically in order to find correlations and trends. Temperatures were measured with a portable pyrometer inside and outside the tafoni. In order to study temporal variations during day–night cycles, we installed two temperature moisture dataloggers (EASYLOG 24RFT, Greisinger electronic GmbH, Regenstadt, Germany) during the summer of 2005. Relative humidity and temperature were monitored from 25 May 2005 to 08 October 2005 inside a tafone and in a well-ventilated fracture, 2 m away from the tafone, on the northern slope of a rock castle at 1755 m a.s.l. (Figure 4).

In a micromorphological approach we analysed 24 thin sections of rock samples taken from the visor of the tafoni. This enabled us to consider petrological differences as well as cementation zones, mineral alteration/weathering and microfractures. As thin sections represent a section normal to the rock surface, the results of weathering processes can be observed. Raster electron microscopy (REM) and coupled energy dispersive X-rays (EDX) were used on four debris samples collected at the top ceiling of a tafone near Calvi (Cal_1). Surface structures of grains visible under the REM give evidence for mechanical (conchoidal fracturing of quartz grains) and chemical weathering (dissolution of mineral grains). EDX allows identification of elements like sulfur or chlorine that might contribute to salt weathering. A LEO scanning microscope (LEO model 1450 VP, LEO Electron Microscopy Ltd, Cambridge, UK) with an Everhart-Thornley SE-detector and a four-quadrant BSE-detector. The coupled EDX system (Oxford Instruments, Oxfordshire, UK) was an Oxford INCA 200 Premium Si (Li) SATW detector. For surface analysis grains were coated with gold while samples for EDX were coated with carbon as the high atomic weight of gold attenuates signals of lighter elements.

The geochemical approach included ^{10}Be dating of the exposed tafoni surfaces at three different locations (Capu Aleri, Bavella and Calvi) representing coastal and inland sites. In order to extract information on the nature and origin of salts involved in the weathering process, quantitative analysis of

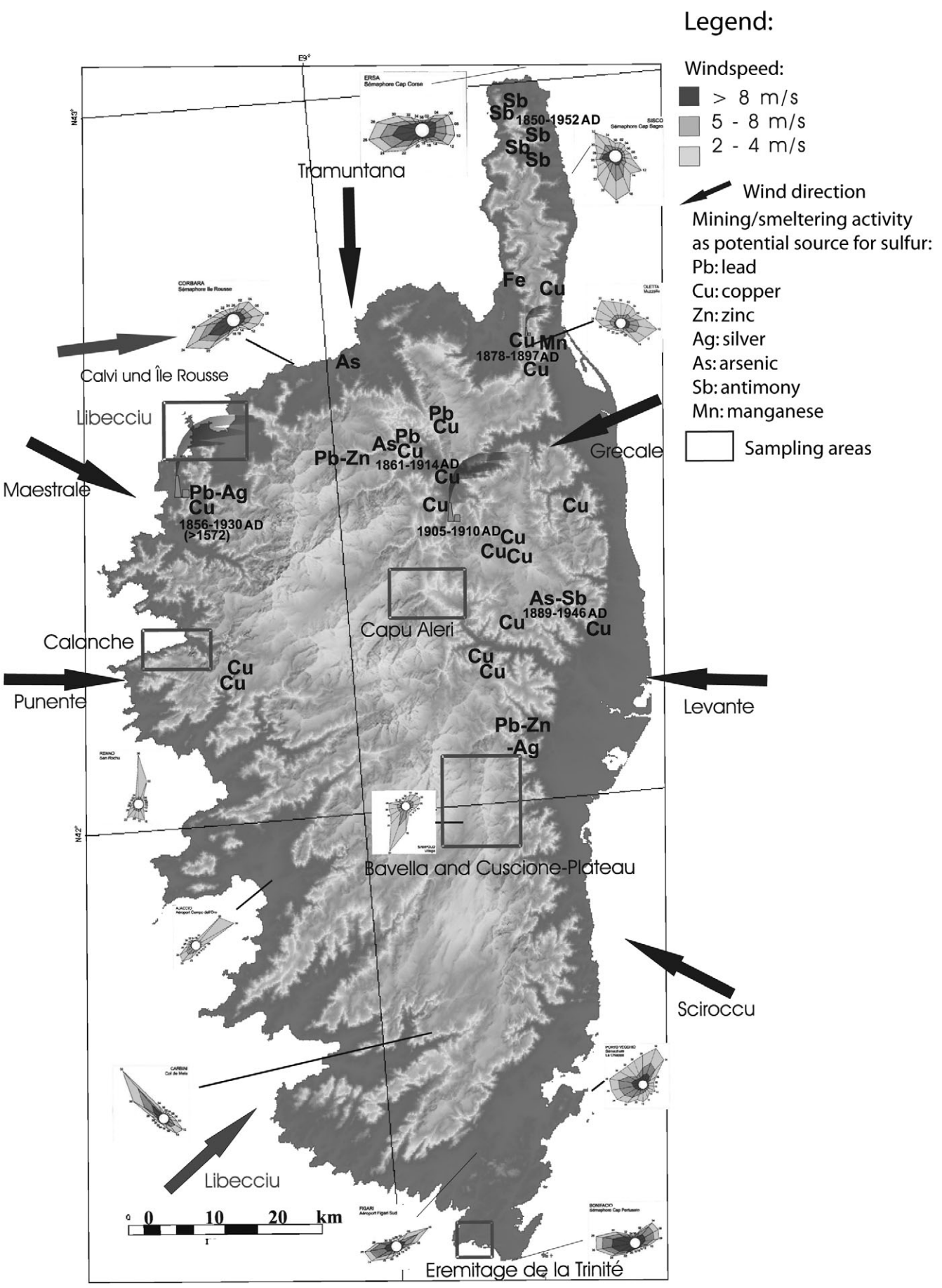

Figure 1. Map of sampling locations, wind directions, ore deposits and smelters as potential sulfur sources.

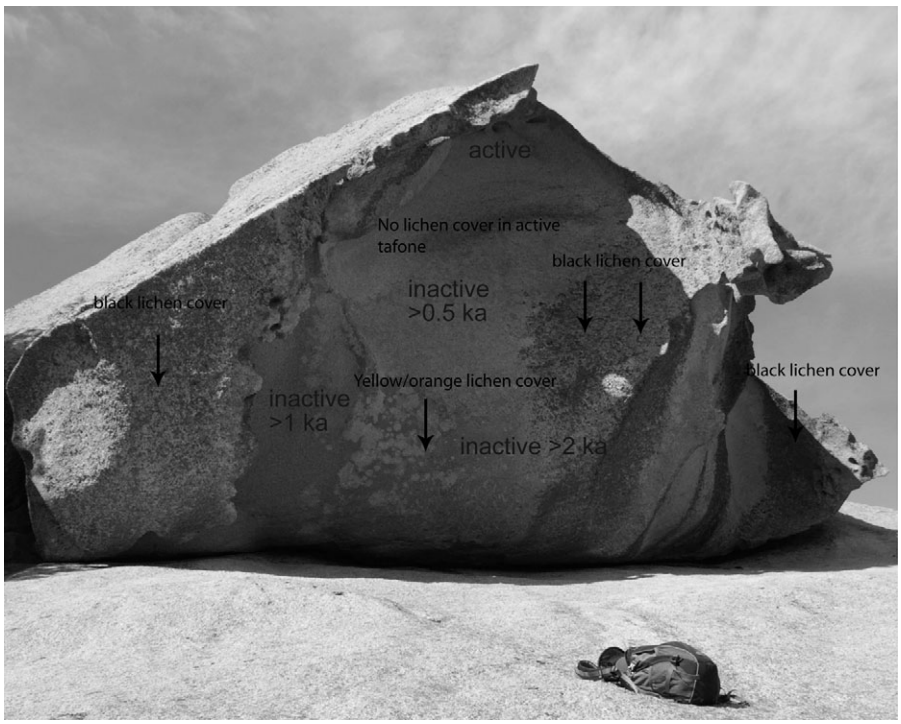

Figure 2. Tafone at Capu Aleri/Pinerole (1620 m a.s.l.), exposed to the south, showing different and colourful lichen cover. Black vertical lichen cover develops from overflowing water, collected in silicate karren and ponds on the top surface of the granite rock castle. Scattered black lichens typically grow where rain can fall on the rock surface. Orange-red lichens are typical of strongly overhanging cliffs. Yellow lichens grow in all local environments here. Maximum size of individual yellow lichens and to some extent overall lichen cover, indicate the time of surface exposure of different segments of the interior. Moisture for lichen growth in strongly overhanging parts is provided by surface condensation from clouds.

ions contained in debris samples was done using ion chromatography. Also the sulfur isotopy of gypsum contained in the samples was measured.

Exposure dating of tafone surfaces with cosmogenic ^{10}Be is based on the assumption that vertical rock surfaces inside a tafone are exposed by a cavity-forming process which mainly moves upward and leaves the newly exposed surface largely unchanged. A decreasing in exposure ages along a vertical profile through a tafone would be expected until sampling approaches the penetration zone of most cosmic rays about 2 m below the top of the overlying granite roof. This certainly is a simplification as the cavity-forming process may start again from the bottom, or continue laterally backward (Matsukura and Matsuoka, 1991). In several cases, however, the state of surface preservation and the local geometry suggest that such modification has not occurred, and consequently such sites were selected for sampling. The three sampled sites show a slight convexity in the central vertical section of the backwall, and the granite lacks any tafone debris, in contrast to the topmost and concave vertical section. Lichen cover inside tafone at Capu Aleri (1620 m a.s.l.) shows that even in the case of a relatively smooth surface the weathering process stopped at different times in the past. Figure 2 shows the lichen-free active part with few honeycombs and lose tafone debris in the topmost section of a south-facing tafone, and a middle section with yellow lichens about 8 cm across below, indicating its inactive state for more than 500 years, according to the regional lichen growth curve for *Rhizocarpon geographica* (Gob *et al*., 2003). Based on the absence of pale-yellowish, ancient generations of this lichen species, we assume that original colonists are observed. Lichen inside inactive Tafoni are typically found at higher elevations, whereas below 800 m a.s.l. they are rare or absent. This reflects that a minimum of moisture supply, either by fog, clouds, or precipitation during windy weather conditions, is required for colonization and survival of lichens. Lichen colonization times inside tafoni are, however, unknown. Below, a plane surface is almost completely covered by orange-red, fast growing lichens and yellow lichens up to 14 cm across, among the largest individuals in Corsica, suggesting a minimum age of roughly 2500 years, calibrated on a ^{10}Be-dated rockfall deposit in Corsica (unpublished own data). Left aside of this surface less dense lichen cover indicated less favourable environment for lichens with diameters up to 10 cm, indicating an inactive state for about 1000 years. Hence, inside geometry and lichen cover both indicate active Tafoni formation in segments. Exposure dating of a tafone interior surface would therefore constrain the latest weathering activity on a particular segment. Time-integrating 'average' growth rates of large tafoni are expected to scatter highly as the segments are large.

Samples for exposure dating were taken from the topmost centimetre of the tafone wall resulting in quartz samples of 12 to 36 g that were prepared in Tübingen for accelerator mass spectrometry (AMS) at the ETH facility in Zurich. Mineral separation generally followed the procedure of Kohl and Nishiizumi (1992) and the Be was extracted following von Blanckenburg *et al*. (2004). Originally, the measured ^{10}Be/^{9}Be ratios were normalized to the standard S555 with a nominal value of $95{\cdot}5^{-12}$ using a ^{10}Be half-life of 1·51 Myr. Since Korschinek *et al*. (2010) and Chmeleff *et al*. (2010) recommend the use of a new ^{10}Be half-life of 1·387 Myr and subsequently the in-house AMS Be standards in Zurich were re-evaluated, we converted the AMS measurement data of the tafoni samples to the new system following Kubik and Christl (2010) and Kubik *et al*. (2009) to allow for better comparisons with AMS results from other laboratories.

For the calculation of exposure ages and erosion rates we used the CRONUS-Earth online calculator (http://hess.ess.washington.edu/), version 2·2 (Balco *et al*., 2008 and references therein). The new half-life is incorporated into this version and normalization of the measurements is taken into account. The calculator uses the value of 160 g cm^{-2} for the attenuation length of production by spallation. Local surface production rates are scaled after Stone (2000). From the five offered scaling schemes for spallogenic production we chose the one after Dunai (2001) where cutoff rigidity and atmospheric pressure determine the scaling factor and the production rate is corrected for magnetic field changes through time. Hence, the production rate for spallation is $4{\cdot}9 \pm 0{\cdot}56$ at g^{-1} yr^{-1} (Balco *et al*., 2008). The exposure ages are

calculated under the assumption of zero erosion. Local production rates are uniformly corrected for sample thickness, by multiplication by a factor 0·9916. The samples from inside the tafone have quite strong local topographic shielding as the sample position is always at a vertical rock wall and also under a visor. This kind of sampling site with a highly complex individual geometry pushes the method to its limits as it works best for horizontal unshielded surfaces. As the final goal is to compare trends of weathering rates we consider the cosmogenic dating an appropriate tool, even when using a simplified vertical exposure approach.

In order to quantify solute material and to identify different salt species in the weathered rocks, we took debris samples from the ceiling, the back wall and the floor of 100 tafoni, distinguishing between coastal sites and mountain tafoni of the interior. The samples were carefully ground to grain size smaller than 3 mm and put into ultrapure water and left on a shaking-table for 12 h. After filtering, concentrations of ions were measured with an ion chromatograph DX 120 in Tübingen.

As sulfur proved to be an important constituent of the ions, we evaporated a solution of 134 g of debris in 67 mL ultrapure water from two samples (Calvi and Capu Aleri) and analysed the resulting crystals using XRD (Bruker D8-GADDS with Microdiffractometer, Eulerwiege and UMC-stage). Organic substances in the solute were removed by filtering. Evaporation temperature was 150°C.

Sulfur contained in these crystals (mainly gypsum) was isotopically analysed with a Carlo Erba element analyser (CE 2500) coupled with a Finnigan MAT Delta Plus XL mass spectrometer after the method of Giesemann *et al*. (1994). Samples were reacted in a He carrier together with an oxygen spike at 1050°C. The resulting SO_2 was separated and SO_3 was oxidized by contact with metallic copper at 650°C to SO_2. Final results were calibrated to international standards (IAEA S1 to S3 and NBS 123) with values of –0·3, –32·1 and 17·1 ‰, respectively.

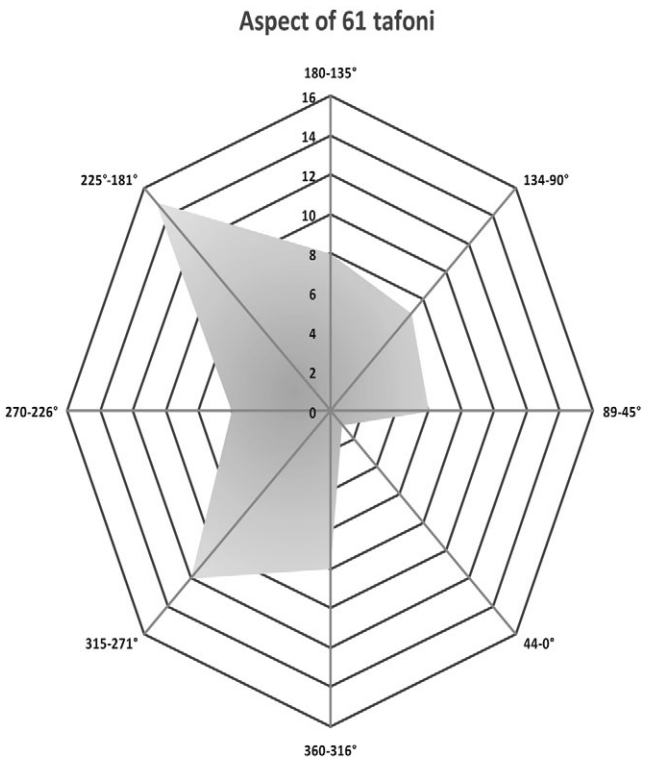

Figure 3. Aspects of 61 documented tafoni, revealing a lack of tafoni in the south-east quadrant.

Results

Geomorphology

The data collected show that the aspect of tafoni follows the local cleavage and fault systems, but also shows two preferential orientations, 181° to 225° and 271° to 315°, the SW and NW quadrants, respectively (Figure 3). These are related to the dominant directions of wind and maximum insulation. Tafoni of Calvi, Calanche and Eremitage de la Trinité at low elevation belong to the first group, while those of Capu Aleri and the Cuscione plateau in the moutainous interior mainly belong to the second group.

Statistical analysis shows no relation between altitude above sea level, distance to the sea and size of the weathering form.

Micro-climate on a temporal scale

The temperature record of the outside data logger reflects a typical Mediterranean summer with few invasions of cool air, typically followed by insulation-driven recovery of normal temperatures at the end of July (Figure 4). The decrease of temperature and its daily amplitude are clearly visible.

We extracted three typical episodes of insulation-driven warming (Figure 4; 26–30 May, 17–21 June, 25–29 July) to show daily amplitudes in fair weather conditions (weak SW to SE winds). The episodes of 7–11 July and 2–6 October show cool periods with winds from NW to N, the latter episode with strong winds. Inside the tafone, the average summer temperature (25 May–6 October 2005) is about 1·4°C higher than outside in free air during calm insulation periods and cool summer phases. Cool and windy October conditions minimize this temperature difference. A plot of humidity would look much the same, with on average about 9% drier conditions inside the tafone during the entire measurement period.

The daily temperature range during insulation periods shows a time lag between the maxima and minima inside and outside the tafone. Outside, the minima occur at sunrise, inside between 11:00 and 12:30 UTC. Maxima on the north-facing slope occur later than in an open area (15:00–16:00 UTC) between 18:00 and 19:00 UTC because of local upward-directed winds. Inside, maxima occur after midnight. Hence, inside the tafone temperature has a time lag of 4 to 7 h, certainly depending on the geometry of the tafone and the distance to the top outside surface. The larger this distance, the more time passes before either the daily insulation heat wave or radiative cooling at night modify the temperature by conduction through the granite.

The data show that capillary transport of moisture inside the granite is driven not only by insulation on top but also by dry and warm conditions inside the tafone at night. The effect inside is strongest in the absence of wind, as the warm air in the tafone is allowed to move up and to be stored inside, like in a balloon. As a result, capillary upward movement until the evening of sunny days is expected to change to lateral movement in the following nights, towards the tafone back wall and top. We have no further evidence to support this expectation or to discuss possible consequences for the shaping of tafoni over long timescales.

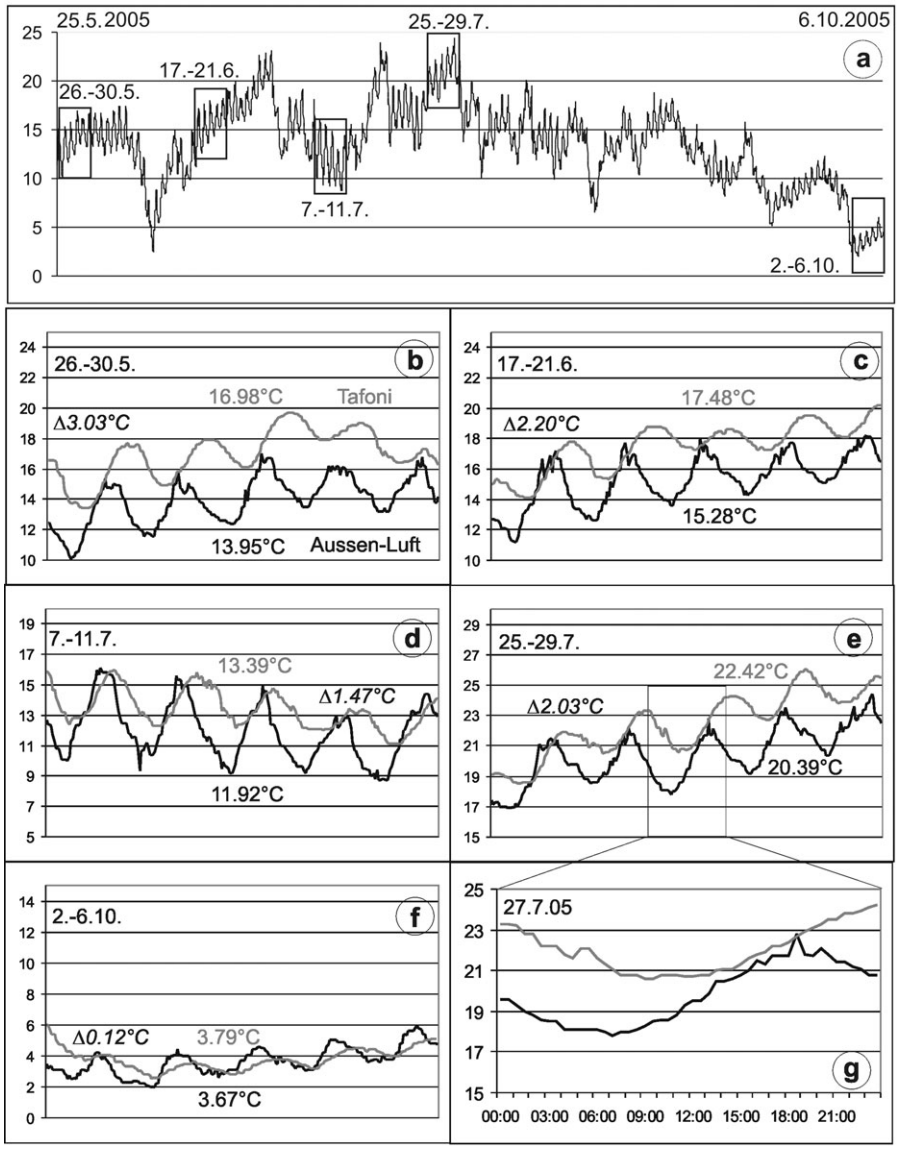

Figure 4. Microclimate inside and outside a north-facing tafone at 1755 m altitude in north-central Corsica (Pinerole) during summer (25 May–6 October 2005). The outside temperature record (a) shows typical 5-day weather periods (b) to (f) in which inside and outside tafone temperatures are compared. Figures (b), (c) and (e) show fair weather periods of weak winds and normal (c) or elevated ((b) and (e)) seasonal temperatures. The maximum temperature difference between inside and outside, and intra-day offset is observed during the time of maximum insulation. In seasonally cool periods (d) with occasional clouds and some wind the temperature difference is somewhat smaller. In cool cloudy and windy autumn periods (f) there is hardly any inside and outside temperature difference. The time offset of daily minima and maxima inside and outside the tafone, in the range of several hours, is shown for the hottest time period of that summer (g).

In-situ pyrometer measurements of spatial temperature distribution inside tafoni

Measurements of radiant temperature inside the tafone and on the outer surface in May 2008 mostly showed slightly higher temperatures on the outside walls, especially on days with high insulation (Figure 5). The mean temperature difference is 1·87°C while the maximum reaches 7°C on a windy and sunny day at noon, with a minimum of 0°C on a rainy day. Radiant temperature is dependent on the lithology as emissivity and transmission of heat are variable for different minerals. Considering the spatial temperature distribution inside a single tafone, it becomes clear that highest temperatures prevail near the top (rock surface orthogonal to the sun during direct insulation) while lowest temperatures were recorded at the base of the structure.

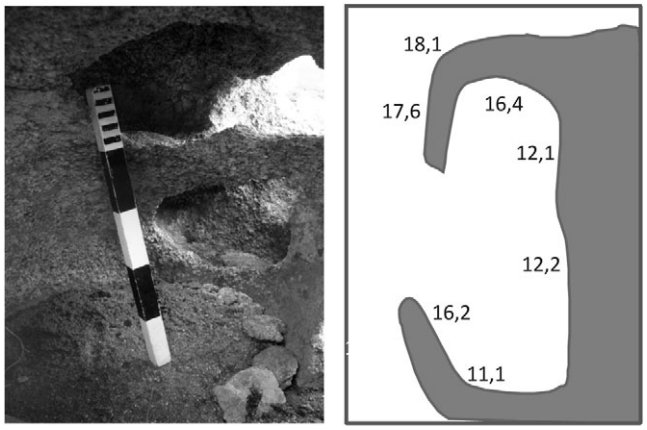

Figure 5. Temperature distribution inside a tafone near Fughiccia (square section of the cavern illustrated in the photo, which is open on both sides or linked to other caverns). Values are in °C and were obtained with an infrared pyrometer at 1 PM on a sunny day with sporadic cloud cover. Note temperature differences from top to bottom of the cavern.

Micromorphology: crystal-scale features (thin sections and REM)

The rocks considered are either subalkaline granitoids or alkaline granites of Variscan or Permian age, respectively. Epithermal alteration occurred during Alpine orogenesis. Some rocks like those at Eremitage de la Trinité are relatively unaltered

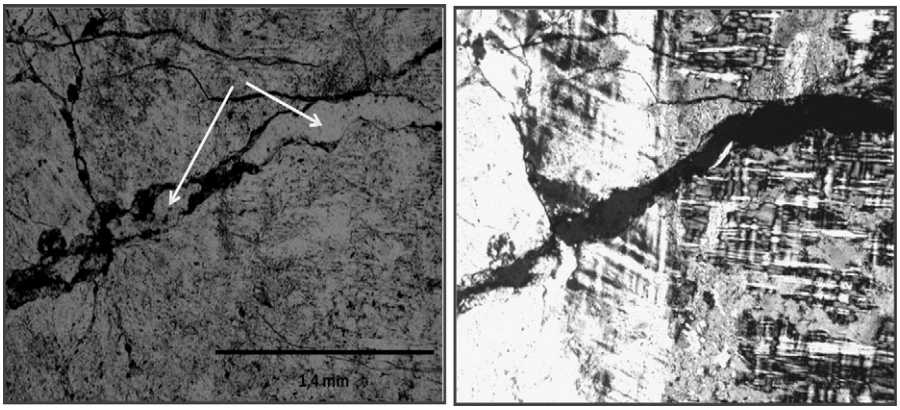

Figure 6. Thin section of a granodiorite of Capu Aleri. On the right: X Pol, on the left: II Pol. Secondary silicification in micro-fractures and weak sericitization and kaolinitization in the microcline are visible.

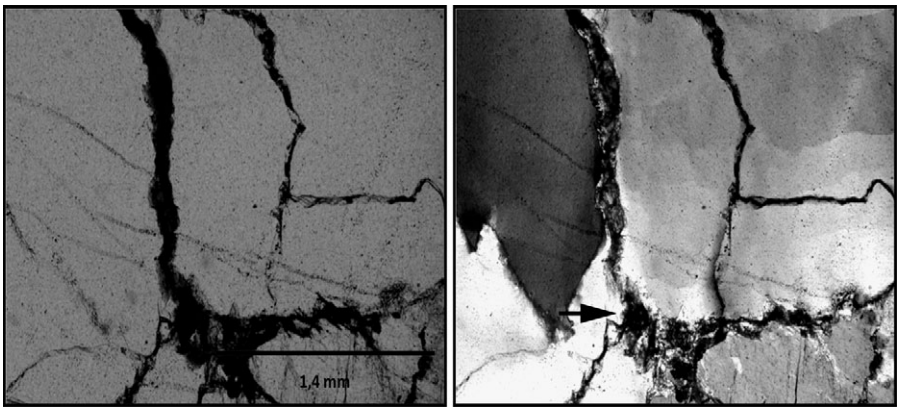

Figure 7. Thin section of a granodiorite of Capu Aleri. On the right: X Pol, on the left: II Pol. Cementation of micro-fractures by iron oxides and hydoxides is clearly visible.

while other rocks such as those at Capu Aleri show hydrothermal alteration, cementation, and micro-fracturing. Thin sections were taken from the visors to show a profile from the outside toward the inside of the rock.

We found indications that differences in lithology, microfracturing, alteration and cementation modify weathering rates but were not able to quantify the impact. For instance, a high proportion of feldspar and biotite aparently leads to higher weathering rates than observed in quartz-dominated rocks under otherwise constant conditions because feldspars are less resistant to weathering. Microfracturing as observed at Capu Aleri appears to increase weathering rates. By contrast, secondary hydrothermal silicification increases weathering resistance (Kuhlemann *et al*., 2008).

Cementation zones of iron-oxides/-hydroxides at rain-exposed top surfaces, sampled at visors, enhance resistance to weathering processes. In the case of Capu Aleri we found both microfractures and mineral-alteration (chloritization of biotite, sericitization and kaolinitization of feldspar) as well as cementation zones and hydrothermal silicification.

On the outside of the visor we observed micro-fractures and corrosion of single grains. Lichen cover locally modifies weathering, involving both, mechanical and chemical processes. Mechanical weathering is caused by penetration of the hyphae through cleavage planes and fractures as well as by the expansion and contraction of the thallus associated with its hydration state. Lichen acids are the reason for chemical weathering. As lichens need stable surfaces for colonization, they are an indicator of inactive tafoni, but contribute, as described above, to the weathering of the outside surfaces.

As micro-fractures can be observed not only on the rims but also throughout the thin sections, they originate from other processes such as metamorphic deformation and salt crystallization. Permeability and porosity are two important parameters for weathering as the transport and the crystallization of salts are dependent on these factors. It was shown by Rivas *et al*. (2003) and Goudie and Viles (1995), that the properties of the circulating solution and the duration of drying cycles are important for the magnitude of weathering by salt crystallization, and, as a whole, these parameters control the depth of the weathering front and thus the type of debris obtained, ranging from small flakes to large scales.

Analysis of debris samples from a tafone near Calvi (Cal_1) by REM and EDX showed fracturing of mineral grains in all samples, which is a strong indicator for mechanical weathering. We found little evidence for chemical weathering (Figure 8).

Out of 106 EDX spectra sulfur was detected in only two cases (0·09 at%) and chloride in three cases with a maximum of 3·3 at%.

There is strong evidence for bacterial activity as shown in Figure 9. It is most likely that the iron-oxidizing, aerobe bacteria Leptothrix is involved in building pipes of iron-bearing minerals. These bacteria occur under neutral pH conditions and use oxygen as electron acceptor for encymatic oxidation of Fe(II). They form tubelike layers which are coated with iron-bearing minerals. It was suggested that the excretion of iron prevents crustification of the Fe(II)-metabolizing cells that would hinder substrate absorption and metabolite execretion and even lead to the death of the cells (Kappler and Straub, 2005).

Geochemistry

Geochemical data of solute material

The results of ion chromatography show high sulfate, calcium, chloride and sodium concentrations in debris samples, especially in samples from the upper wall and ceiling of tafoni (Table I). Whole-rock samples that were ground and analysed

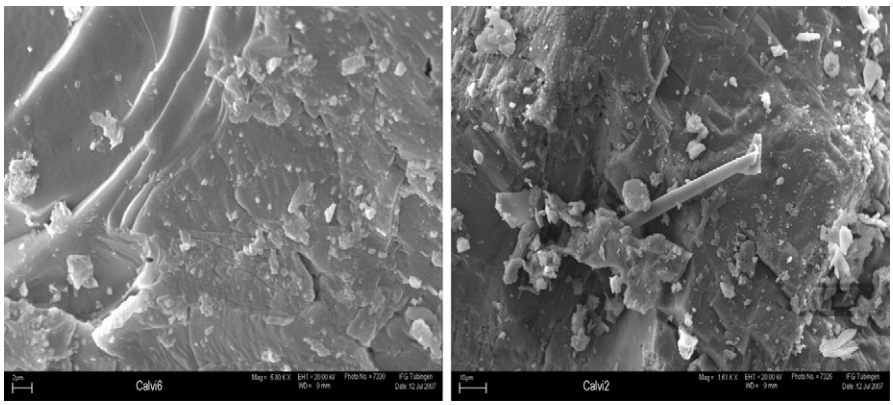

Figure 8. Fractured mineral grains indicate mechanical weathering.

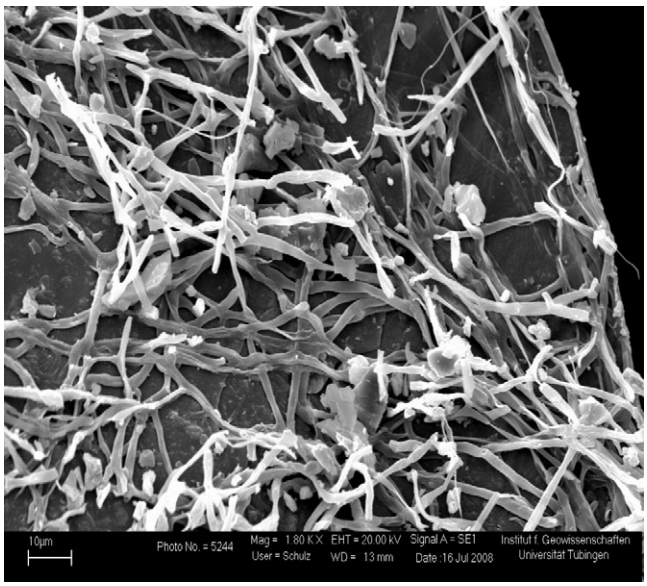

Figure 9. Evidence of bacterial presence.

in the same way as the other samples show generally low concentrations and little variations. Samples from ceilings show highly variable SO_4, Ca, Cl, and Na concentrations and little variations in the other measured ions except for bromide, which varies strongly in all samples. Values up to 18·4 µmol L^{-1} sulphate were observed in ceiling samples whereas 1·5 µmol L^{-1} occur in whole-rock reference samples. Mean values are 6·4 µmol L^{-1} and 0·37 µmol L^{-1}, respectively. Obviously, salt is enriched in the debris samples. Coastal tafoni in particular show high salt concentrations and suggest that sea-salt is an important component of the salt. A significant correlation was found between sulfate and calcium, and chloride and potassium, suggesting that gypsum and halite are dominant minerals (Figures 10 and 11).

Apart from sea-salt we consider other potential sources for salt-forming ions involved in tafone weathering. High sulfate and calcium concentrations indicate gypsum and to a minor amount mirabilite and thenardite, two very destructive sodium sulfates as further minerals in addition to sea-salt derived halite. This finding suggests that sea-salt cannot be the only end-member as sulfur and calcium dominate significantly and the deficit of halite-forming ions in the samples cannot be explained by a higher mobilitiy within the relatively dry and protected caverns. As potential sources of sulfur we consider (1) the sulfide minerals within the rocks, (2) volcanic input from Italy (so-called 'dry-fogs' described by Camuffo and Enzi (1994), (3) modification by elements contained in circulating local water, (4) anthropogenic sulfur contained in air masses from Europe and deposited by precipitation might be of some importance but only since the beginning of industrialization in Europe in the 18th century, (5) Saharan dust-input by dry and wet deposition as described by Loye-Pilot and Martin (1996).

Measurements of $\delta^{34}S$ show that options 1 to 4 can be dismissed as gypsum derived from debris samples has values of 17–19‰ in comparison with 0–5‰ for anthropogenic sulfur, around 7‰ for sulfur from pyrite-weathering and –3 to 10‰ for volcanic ashes (Querol *et al*., 2000; Dünkel, 2002; Bao *et al*., 2004). The values suggest Sahara dust as the major source apart from sea-salt as Cretaceous and Cenozoic marine evaporites with similar values are exposed in the northern Sahara.

Comparison of element ratios calculated from concentrations in our samples with ratios published by Loye-Pilot and Martin (1988) and calculated from concentrations in sea water and local mineral water (Zilia) shows at least three major sources (Figures 12 and 13). Data from Loye-Pilot and Martin (1988) present element concentrations of precipitation of different air-mass situations in Corsica. Air masses from north Africa are rich in Saharan dust while air masses from Europe show anthropogenic contamination in the form of high sulfur concentrations.

Cluster analysis of the element ratios Cl/SO_4, Na/Ca, Ca/K, SO_4/Ca, NO_3/Ca with SPSS and subsequent comparison of the obtained three major cluster centers with the above mentioned ratios shows that most samples fall into a cluster representing a mixture of air masses (Table II). As tafoni are significantly older than anthropogenic sulfur emission, it should not be considered as an essential source, although they are capable of causing a modification of total concentrations during the past 200 years. High concentration of gypsum in Saharan dust seems to be an important end member. This hypothesis is strengthened by the results of sulfur isotopy as in northern Africa many exposed sediments are of marine origin and have similar $\delta^{34}S$ values.

Cosmogenic nuclides

The first sampling site for exposure dating is located in south-eastern Corsica at 510 m a.s.l. Advection of clouds and sea spray to this small intramontane depression is hampered by a mountain range with altitudes between 1100 and 1350 m. Two samples from the inside yielded exposure ages of 3·2 kyr (Taf-1) for the upper segment and 21·2 kyr (Taf-2) for the lower segment (Table III; Figure 14). In the upper sampling position, nuclide production by cosmic rays penetrating the roof of the rock castle, some 0·6 m below the present top, should be important, as the distance matches half the attenuation length (Figure 14). Surprisingly, the ^{10}Be concentration is low and the apparent exposure age young. The silica-karstified surface of the top makes shielding by further rock cover unlikely for the

Table I. Descriptive statistics of element concentrations in 100 samples. Values are calculated from concentrations [µmol L^{-1}]

ID	Mean	Median	Min	Max	Standard deviation	Variance
Fluoride	0·176345606	0·037957501	0·002242796	2·534027243	0·425058964	0·180675123
Chloride	2·214040918	0·842809832	0·009815356	23·60715407	3·787162135	14·34259704
Nitrite	0·012703827	0·00434683	8·98398E-05	0·178917206	0·025140885	0·000632064
Bromide	0·001327966	0·001250132	2·58613E-05	0·00920376	0·001041913	1·08558E-06
Nitrate	0·312003597	0·168084677	0·001612903	2·230993548	0·378199915	0·143035175
Phosphate	0·019396268	0·002102657	4·35014E-05	0·489573705	0·062344229	0·003886803
Sulfate	3·246029641	0·674143994	0·010085839	18·39585568	5·04508401	25·45287266
Sodium	2·373444488	1·187769166	0·028316363	22·683898	3·444522386	11·86473447
Ammonium	0·140546502	0·106578423	0·001972814	0·930912304	0·140303728	0·019685136
Potassium	0·295920417	0·170172734	0·001801868	3·395563212	0·444342404	0·197440172
Magnesium	0·522461975	0·212706755	0·002750841	4·117713613	0·737063561	0·543262694
Calcium	3·145796903	0·517762964	0·016759522	17·46062793	4·896442137	23·9751456
Reference samples						
Fluoride	0·662405034	0·118022164	0·006351686	2·534027243	1·04958594	1·101630646
Chloride	0·355721188	0·219421454	0·027484585	0·834152723	0·304191776	0·092532636
Nitrite	0·012807299	0·004345643	0·004337177	0·06383276	0·019817081	0·000392717
Bromide	0·001375235	0·001250906	0·001248499	0·002287155	0·00031619	9·99762E-08
Nitrate	0·10804086	0·039557258	0·007840323	0·519620968	0·153918348	0·023690858
Phosphate	0·002607384	0·001052894	0·001050583	0·01337138	0·003491818	1·21928E-05
Sulfate	0·37668073	0·152680752	0·016081223	1·452067173	0·470922099	0·221767623
Sodium	0·78405021	0·69786925	0·126737963	1·960368721	0·597515297	0·35702453
Ammonium	0·043428278	0·02188023	0·003573858	0·185452957	0·052089607	0·002713327
Potassium	0·12656623	0·125104373	0·022852804	0·39411521	0·1078935	0·011641007
Magnesium	0·080514019	0·032546957	0·002750841	0·408019203	0·121694588	0·014809573
Calcium	0·31250322	0·12337262	0·016759522	1·007022477	0·378291356	0·14310435
Samples from the ceiling						
Fluoride	0·157107286	0·049180166	0·005600385	0·872596076	0·23926478	0·057247635
Chloride	2·254305743	0·883728862	0·009815356	11·17078277	2·725060978	7·425957332
Nitrite	0·018385456	0·004344228	0·001645822	0·178917206	0·039839321	0·001587172
Bromide	0·001445659	0·00125028	0·000473766	0·004844139	0·000932953	8·70401E-07
Nitrate	0·401324645	0·239540323	0·001612903	2·230993548	0·52718852	0·277927736
Phosphate	0·032407923	0·002100726	0·000926432	0·489573705	0·106229044	0·01128461
Sulfate	6·456377473	3·780594829	0·010085839	18·39585568	6·943906563	48·21783835
Sodium	2·509522389	1·47777246	0·028316363	8·413197865	2·441506575	5·960954356
Ammonium	0·198864116	0·145131731	0·012120008	0·930912304	0·188435157	0·035507808
Potassium	0·333239578	0·262118749	0·024404632	1·766165753	0·36951638	0·136542355
Magnesium	0·649114275	0·346189323	0·004111003	2·412911686	0·708066291	0·501357872
Calcium	6·306482576	3·416752884	0·090201995	17·46062793	6·769055178	45·820108

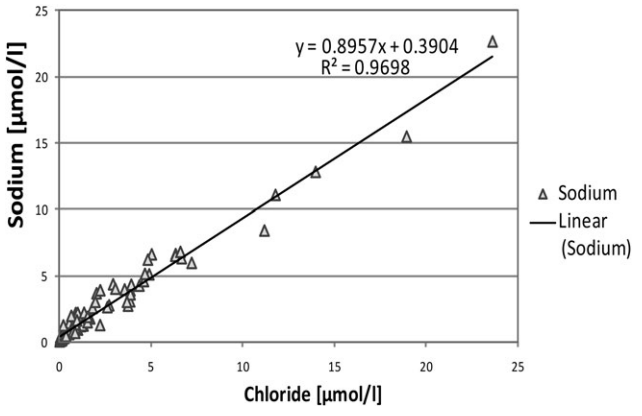

Figure 10. Correlation between sodium and chloride in 100 debris samples.

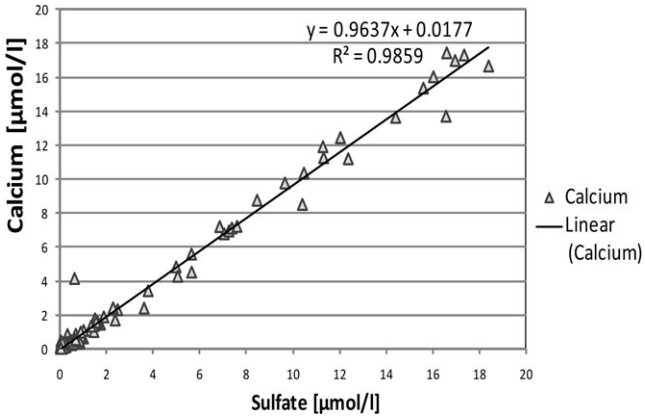

Figure 11. Correlation between calcium and sulfate in 100 debris samples.

last 3 kyr. Instead, we assume that the visor extended much further down, enhancing local shielding, and broke off several centuries ago (Figure 14), and that the tafoni weathering process is quite active in this segment. Unfortunately, this assumption cannot be verified. Active weathering of the lower segment appears to have ended by the end of the Last Glacial Maximum (sample Taf-2). Hence, the tafone segment above (1·6 m high) developed by an average weathering rate of ~75 mm kyr^{-1}, in terms of upward migration. This tendency of upward tafoni growth can be explained by a mechanism described by Hunink *et al*. (2004). Longer drying rates cause the evaporation front to lose contact with parts of the rock

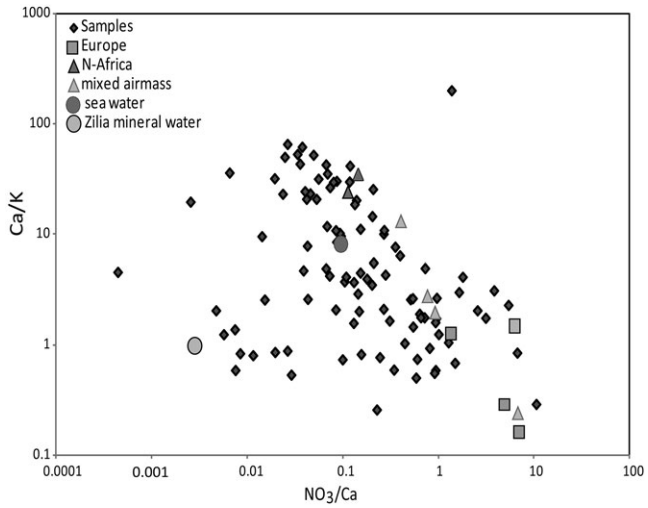

Figure 12. Characterization of end members of salt involved in weathering processes. Element ratios were calculated from values of 100 debris samples and plotted together with typical values for sea water (White, 2005), values calculated from the concentrations in local mineral water (Zilia) and published data (Loye-Pilot, 1988) for precipitation out of different air-mass situations (Europe, N-Africa, mixed).

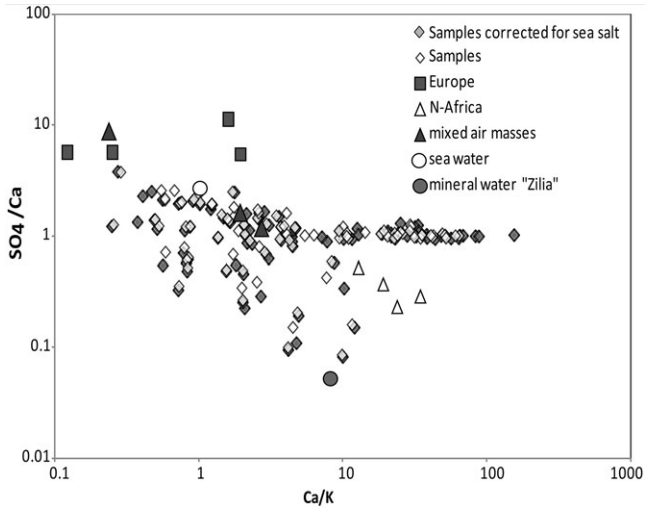

Figure 13. Characterization of end members of salt involved in weathering processes. Element ratios were calculated from values of 100 debris samples and plotted together with typical values for sea water (White, 2005), values calculated from the concentrations in local mineral water (Zilia) and published data (Loye-Pilot, 1988) for precipitation out of different air-mass situations (Europe, North Africa, mixed). For samples corrected for sea-salt, concentrations were corrected according to NaCl contained in the samples because sea water is the main source of these elements.

surface and most salt crystallizes in the sheltered parts of the rock surface (under the sheltered ceiling). Therefore fast weathering can be observed in these parts. As shown in Figure 14, the tafone is about 1·5 m wide and more than 0·5 m deep, and hence a volume of about 1 m^3 of granite has been weathered (~25 mm^3 yr^{-1} on a surface of ~1 m^2).

The exposure dating at the foot, on a 20° east-dipping surface, yielded 13·0 kyr (Taf-3). An older age than for sample Taf-2 was initially expected, because this sampling position was expected to be exposed during formation of the lower segment. It seems that the sampled site was protected by a granite desquamation plate, part of which is still close to the original position, slipped off during termination of glacial times.

Table II. Solution of a hierarchical cluster analysis of element ratios compared with values calculated from concentrations in precipitation (Loye-Pilot, 1988)

Cluster centers of final solution			
Cluster	N-Africa	Mixed aimasses with high EU component	Europe (strong marine influence)
Cl/SO4	0·308680139	2·066097865	13·20968347
Na/Ca	0·365870964	3·102977995	30·09793134
Ca/K	37·50152405	4·717354783	1·185214783
SO4/Ca	1·030571229	1·105515002	2·399800432
NO3/Ca	0·308787441	0·690155162	0·619988998
Na/Ca	0·365870964	3·102977995	30·09793134
Number of cases:	20	74	5

The second sampling site south of Calvi is strongly exposed to sea spray, as testified by salt-tolerant vegetation (Figure 15). Tafone weathering activity below the roof was very active, as testified by a centimetre-thick active layer with honeycomb structures. Unfortunately, the measurements of samples Taf-4 and 6 failed, and only one sample from the inside was successfully measured, yielding the quite high exposure age of 69 kyr (Taf-5, Table III). This age suggests that the tafone started to form in the last interglacial with an upward weathering rate in the range 40 mm kyr^{-1} in this individual head-shaped tafone. The volume of about 8 m^3 is high but the weathering rate (~14 mm^3 yr^{-1} on a surface of ~1 m^2) is lower than in south-eastern Corsica, both with respect to upward migration and volume. It is, however, expected that the weathering rate decreases with increasing size of the tafoni.

Sample Taf-8, fully hidden from direct cosmic rays under the visor, has about 0·7 m of vertical distance to the top (Figure 15), which means that all cosmogenic ^{10}Be production originates from cosmic ray penetration through the granite roof, across the given fairly irregular shielding geometry. The ^{10}Be concentration at the top surface (Taf-7) reflects an average weathering rate of about 12·5 mm kyr^{-1}. This weathering rate is quite high compared with those observed at subalpine elevations (Kuhlemann *et al.*, 2008).

The last sampling site is situated in the Pinerole massif in the dry northern centre of Corsica. It is a granite cupola with a silica-karstified top and mid-sized Tafoni on most sides (Figure 16). A plane surface between potholes on the top yielded an average weathering rate of 5·5 mm kyr^{-1} (Taf-12, Table III). Sample Taf-10 from a granite rib separating a lower and an upper tafone segment yielded an exposure age of 14·3 kyr which would indicate up to 1·7 m of upward weathering since then, equivalent to 135 mm kyr^{-1} (~50 mm^3 yr^{-1} on a surface of ~1 m^2). This weathering rate is high compared with the other two sites. The granite rib is not affected by active tafoni weathering but instead is covered by various types of small lichen. Even more disturbing is the high ^{10}Be concentration in sample Taf-9, which is more than half as high as that on the top (Table III). At a depth of 0·7 m below the top surface, at the given low weathering rate at the top, more than a quarter of the ^{10}Be concentration probably formed by penetration of cosmic rays though the shielding top granite. More than half of the present ^{10}Be concentration in sample Taf-9 might derive from lateral exposure. This would give an exposure age of about 77 kyr, and hence an upward weathering rate of

Table III. Exposure ages and erosion rates for the ^{10}Be samples as calculated by the CRONUS-Earth online calculator (version 2·2)

Sample No	Lat. [°N]	Long. [°E]	Alt [m]	Qz [g]	^{10}Be 10^4 [at g^{-1}]^a	Error (%)	Topogr shield. factor	Local prod. rate [at g^{-1} a^{-1}]	**Age** (years) (Dunai)	**Error** (years)	**Erosion rate** (m Myr^{-1}) (Dunai)	**Error** (m Myr^{-1})
Taf-1	41·82	9·26	512	11·81	1·414	20·8	0·74990	4·95	**3200**	**764**		
Taf-2	41·82	9·26	511	20·02	10·178	7·0	0·74990	4·95	**21286**	**2925**		
Taf-3	41·82	9·26	510	10·97	6·098	18·2	0·74990	4·94	**13076**	**2839**		
Taf-5	42·55	8·82	160	29·07	26·186	5·0	0·77975	3·81	**69206**	**8982**		
Taf-7	42·55	8·82	164	28·21	30·649	3·4	0·99808	4·93	*63781*	*7920*	**12·47**	**1·26**
Taf-8	42·55	8·82	162	28·33	11·160	5·3	0·10000	2·45	**44415**	**5787**		
Taf-9	42·31	9·01	1633	36·39	99·567	3·0	0·78405	12·59	**76631**	**9467**		
Taf-10	42·31	9·01	1631	33·88	17·442	5·5	0·78405	12·57	**14291**	**1859**		
Taf-12	42·31	9·01	1634	34·25	187·991	3·0	0·99968	16·2	*113759*	*14184*	**5·54**	**0·66**

30 mm kyr^{-1}, which obviously is not compatible with the former rate at the same site. The only natural explanation for the high ^{10}Be concentration in sample Taf-9 is that just above the sampling spot a deep pothole had existed which strongly reduced the shielding effect of the granite roof. In support of this hypothesis, Figure 16 shows an elliptic skyline above the sampling site of Taf-9. Narrow and deep potholes are frequent on the top surface, and some of them are as deep as 0·5 m.

The age of Taf-10 (14·3 kyr, Table III) may be explained by rejuvenated upward tafoni weathering (note lichen-free granite below the granite rip) and downward weathering by rain. At this site, the geomorphic setting is more complex than assumed during sampling. In view of the results, the tafone shown in Figure 2 would probably have been the better choice. The last example shows that our ^{10}Be dating approach on large tafonis gives ambiguous results on the weathering rates of specific tafone sectors.

Field evidence for tafoni weathering rates is also available from dated or correlated moraine boulders of the Last Glacial Maximum (*ca*. 20 kyr; Kuhlemann *et al*., 2008) which have been subjected to *in situ* tafone weathering at altitudes between 500 m and 1300 m. Several of them have been observed, and the typical tafone size in calc-alkaline boulders was 1 to 1·5 m in both height and width. Hence, growth rates were in the range 50–80 mm kyr^{-1}, if active tafoni formation started after glacier retreat by 18 kyr and continued throughout late glacial cold spells.

Summarizing (see Table IV) exposure dating, we find an apparent qualitative trend of increasing tafoni weathering rates with increasing degree of micro-fracturing, ranging between 40 mm kyr^{-1} at Calvi with hardly any microfracturing (however, high top surface weathering rate) and about 130 mm kyr^{-1} at Pinerole, with strong micro-fracturing close to the Alpine deformation front. A much larger data set would be required to differentiate and quantify the role of micro-fracturing, altitude, climate conditions, lithology, and possibly other factors. It is however evident that tafoni weathering operates about an order of magnitude faster (3 to 25 times) than surface weathering of secondarily cemented granite at the top of the same site. The 1991 equation proposed by Matsukura and Matsuoka and the 1996 equation proposed by Sunamura are based on the depth value only because it is the easiest measurement to replicate and is assumed to be a reasonable indicator for tafoni growth by the authors. However, we found evidence that weathering processes are more active in the sheltered top wall portions of the feature. These findings are supported by the mechanisms proposed by Huinink *et al*. (2004). In terms of weathering rates the situation is very complex and we cannot assume a single 'typical' growth function for various climatic and lithologic settings or even equal growth rates in different parts of the feature. The weathering rates calculated above provide just a range of averages at the given size in quite different climate settings.

Synthesis

Tafone weathering significantly contributes to the regional erosion budget in semi-humid to semi-arid regions as it operates about an order of magnitude faster than weathering on bare rock surfaces, cemented by iron hydroxides. It operates as fast as weathering of granite regolith, which has a high internal surface and is exposed to biochemical weathering (Kuhlemann, 2009) Tafone weathering is probably among the most effective weathering processes operating on surfaces of plutonic rocks such as granite. Airborne sulfates from deserts appear to play a major role in the enhancement of tafoni

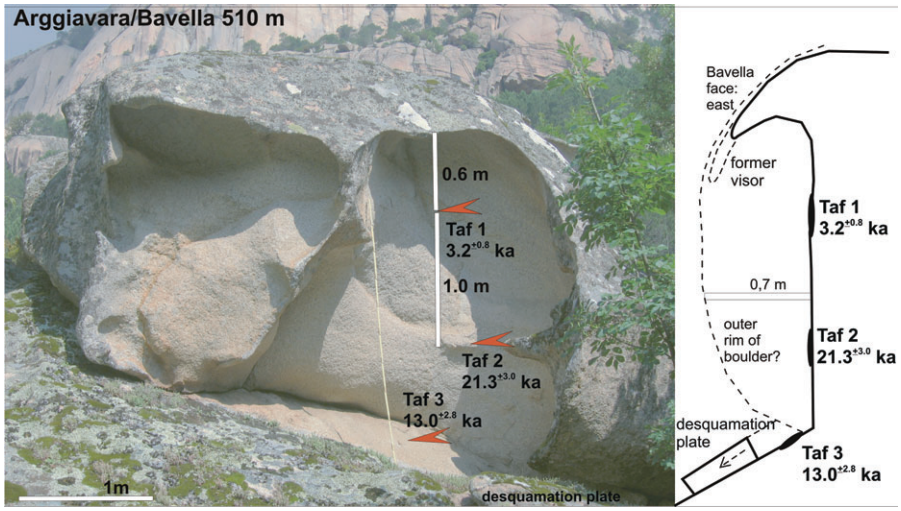

Figure 14. Sampled tafone at the small village of Arggiavara in the northern Bavella massif, south-eastern Corsica. The calc-alkaline granite is the top of a small rock castle, exposed to the east. This figure is available in colour online at wileyonlinelibrary.com/journal/espl

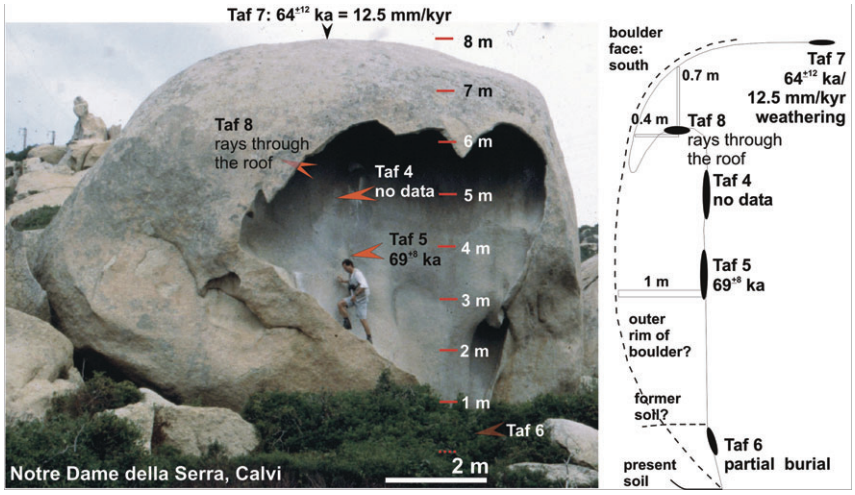

Figure 15. Sampled tafone south of Calvi in north-western Corsica, about 1 km distant from the steep coast. The large boulder is part of a larger field of boulders surrounded by rock castles, all subjected to intense tafone weathering. Several tafoni have already been transformed to tafoni skeletons. The region has been deforested in the last 1000 years. This figure is available in colour online at wileyonlinelibrary.com/journal/espl

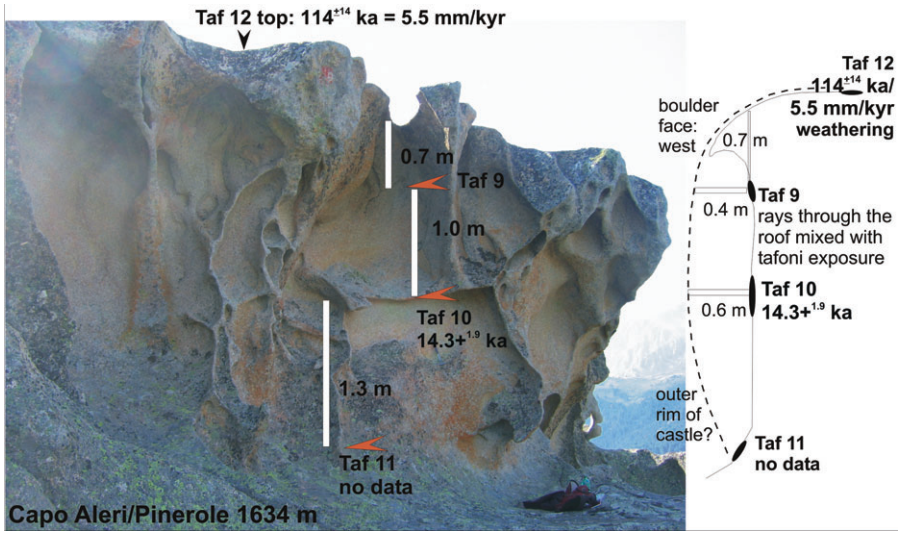

Figure 16. Sampled tafone in northern-central Corsica in the Pinerole massif, representing the centre of Corsica with respect to maximum distance to the coast. This figure is available in colour online at wileyonlinelibrary.com/journal/espl

weathering, and so does industrial sulfur pollution. As tafoni chips are incorporated in the local soil, the salts coating the grains are recycled and the dissolved species are included in the vegetation cycle and eventually move inside the exposed rock to promote further weathering. This means that dust from the deserts not only contributes nutrients directly to soils, but accelerates physical weathering of bare rocks by its salt component, and this way delivers chips of mineral aggregates to the soil. This feedback should be considered for regions where tafoni weathering is common, as well as for global geochemical budgets.

Acknowledgements—Many thanks to Dr H. Taubald who measured sulfur isotopes, E. Reitter and Professor Dr W. Siebel for their support with the laboratory work, Dr C. Berthold for XRF analysis, P. Jeisecke for preparing the thin sections, the whole staff of the laboratory, E. Struve and collegues for ionchromatography measurements, Dr H. Schulz (REM) and B. Neubourg for her help with Be sample

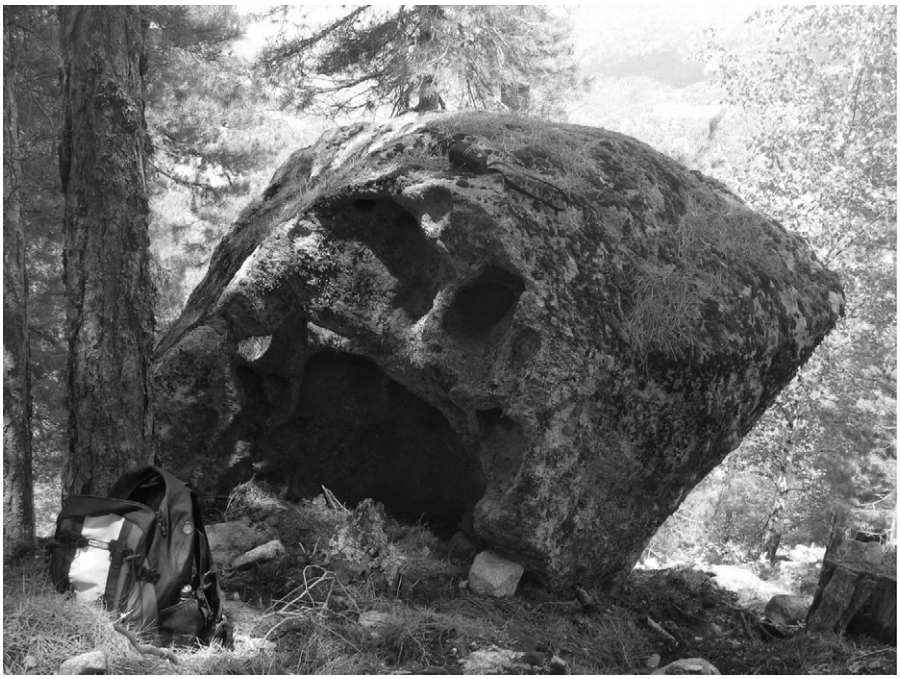

Figure 17. *In situ* formed tafoni in a glacial boulder of a moraine of Last Glacial Maximum age (Kuhlemann *et al*., 2008) in north central Corsica.

Table IV. Summary of weathering rates. Sites represent a transect from the mountainous interior (Pinerole, Bavella) to the coast (Calvi)

Sample	Exposure age [kyr]	Growth rate [mm kyr^{-1}]	r [m]	Volume [m^3]
		Bavella:		
		510 m a.s.l.		
Taf 1	3·2	75	0·7	
Taf 2	21·2			
Taf 3	13			
Top erosion rate				
		Calvi:		
		150 m a.s.l.		
Taf 7 (top)	64	12·5		
Taf 8	175		0·4	
Taf 4	No data			
Taf 5	69	40		8
Taf 6	No data			
		Pinerole:		
		1634 m a.s.l.		
Taf 12 (top)	113	5·54		
Taf 9	76			
Taf 10	14·3			
Taf 11	No data			

Total weathering rates:

	Top weathering rate [mm kyr^{-1}]	Growth rate [mm kyr^{-1}]	Volume growth [mm^3 yr^{-1} m^{-2}]	Total volume [m^3]
Calvi 150 m	12·5	40	14	1
Bavella 510 m	–	75	25	8
Pinerole 1624 m	5·5	135	50	1
glacial boulders		50–80	25–40	0·5

preparation and C. Dörfer for her help during the fieldwork on Corsica. We gratefully acknowledge a very detailed and constructive review by D. Mothershead and a second, anonymus reviewer.

References

Balco G, Stone JO, Lifton NA, Dunai TJ. 2008. A complete and easily accessible means of calculating surface exposure ages or erosion rates from Be-10 and Al-26 measurements. *Quaternary Geochronology* **3**(3): 174–195.

Bao HM, Jenkins KA, Khachaturyan M, Diaz GC. 2004. Different sulfate sources and their post-depositional migration in Atacama soils. *Earth and Planetary Science Letters* **224**(3–4): 577–587.

Blackwelder E. 1990. The hardness of ice. *American Journal of Science* **238**: 61–62.

Bradley WC, Hutton JT, Twidale CR. 1978. Role of salts in development of granitic tafoni, South-Australia. *Journal of Geology* **86**(5): 647–654.

Bruno CDG, Giorgetti J. 2001. Chì tempu face? Météorologie, climat et microclimates de la Corse. CNDP-CRDP de Corse/Meteo France, Ajaccio.

Camuffo D, Enzi S. 1994. Chronology of dry fogs in Italy, 1374–1891. *Theoretical and Applied Climatology* **50**(1–2): 31–33.
Chmeleff J, von Blanckenburg F, Kossert K, Jakob D. 2010. Determination of the ^{10}Be half-life by multicollector ICP-MS and liquid scintillation counting. *Nuclear Instruments and Methods in Physics Research* B **263**: 192–199.
Compton ET. 1892. Vierzehn Tage auf Corsica: Oestereichische Alpen-Zeitung, 347.
Conca JL, Rossman GR. 1982. Case hardening of sandstone. *Geology* **10**(10): 520–523.
Dragovic D. 1969. The origin of cavernous surfaces (tafoni) in granitic rocks of southern South Australia. *Zeitschrift für Geomorphologie* (NF **13**): 163–181.
Dünkel I. 2002. The genesis of East Elba iron ore deposits and their interrelation with Messinian tectonics. Tübinger Geowissenschaftliche Arbeiten (TGA), 65, Tübingen.
Dunai TJ. 2001. Influence of secular variation of the geomagnetic field on production rates of in situ produced cosmogenic nuclides. *Earth and Planetary Science Letters* **193**: 197–212.
Endlicher J. 2000. Mittelmeergebiet. *Regionale Klimatologie* **2**: 153–214.
Giesemann A, Jager HJ, Norman AL, Krouse HP, Brand WA. 1994. Online sulfur-isotope determination using an elemental analyzer coupled to a mass-spectrometer. *Analytical Chemistry* **66**(18): 2816–2819.
Gob F, Petit F, Bravard JP, Ozer A, Gob A. 2003. Lichenometric application to historical and subrecent dynamics and sediment transport of a Corsican stream (Figarella River-France). *Quaternary Science Reviews* **22**(20): 2111–2124.
Goudie AS, Viles HA. 1995. The nature and pattern of debris liberation by salt weathering – a laboratory study. *Earth Surface Processes and Landforms* **20**(5): 437–449.
Guglielmin M, Cannone N, Strini A, Lewkowicz AG. 2005. Biotic and abiotic processes on granite weathering landforms in a cryotic environment, Northern Victoria Land, Antarctica. *Permafrost and Periglacial Processes* **16**(1): 69–85.
Hejl E. 2005. A pictorial study of tafoni development from the 2nd millennium BC. *Geomorphology* **64**: 87–95.
Huinink HP, Pel L, Kopinga K. 2004. Simulating the growth of tafoni. *Earth Surface Processes and Landforms* **29**(10): 1225–1233.
Kappler AS, Straub KL. 2005. Geomicrobiological cycling of iron: molecular geomicrobiology. *Mineralogical Society of America Geochemical Society* **59**: 85–108.
Kelletat D. 1980. Formenschatz und prozessgefüge des"Biokarstes" and der küeste von Nordost-Mallorca (CalaGuya). *Berliner Geographische Studien* **7**: 99–113.
Kejonen AK, Lahti S. 1988. Cavernous weathering forms in Finland. *Geografiska Annaler Series a – Physical Geography* **70A**(4): 315–321.
Kohl CP, Nishiizumi K. 1992. Chemical isolation of quartz for measurement of in-situ produced cosmogenic nuclides. *Geochimica et Cosmochimica Acta* **56**: 3583–3587.
Korschinek G, Bergmaier A, Faestermann T, Gerstmann UC, Knie K, Rugel G, Wallner A, Dillmann I, Dollinger G, Lierse von Gestomski Ch, Kossert K, Maiti M, Poutivtsev M, Remmert A. 2010. A new value for the half-life of ^{10}Be by heavy-ion elastic recoil detection and liquid scintillation counting. *Nuclear Instruments and Methods in Physics Research* B**268**:187–191.
Kubik PW, Christl M. 2010. 10Be and 26Al measurements at the Zurich 6 MV Tandem AMS facility. *Nuclear Instruments and Methods in Physics Research* B**268**: 880–883.
Kubik PW, Christl M, Alfimov V. 2009. New primary 10Be standard and T1/2 for AMS at ETH; recalibration of the in-house 10Be standards. Laboratory of Ion Beam Physics Annual Report.
Kuhlemann J. 2009. Geological Society of London Special Publications 324: 217–235.
Kuhlemann J, van der Borg K, Bons PD, Danisik M, Frisch W. 2008. Erosion rates on subalpine paleosurfaces in the western Mediterranean by in-situ Be-10 concentrations in granites: implications for surface processes and long-term landscape evolution in Corsica (France). *International Journal of Earth Sciences* **97**(3): 549–564.
Loye-Pilot MD, Martin MJ. 1988. Fluctuations of ionic composition of precipitations collected in Corsica related to changes in the origins of incoming aerosols. *Journal of Aerosol Science* **19**(5): 577–585.
Loye-Pilot MD, Martin MJ. 1996. Saharan dust input to the western Mediterranean: an eleven years record in Corsica: the impact of desert dust across the Mediterranean. In *The Impact of Desert Dust Across the Mediterranean*, Guerzoni S, Chester R (eds). Kluwer: 191–199.
Matsukura Y, Matsuoka N. 1991. Rates of tafoni weathering on uplifted shore platforms in Nojima-Zaki, Boso Peninsula, Japan. *Earth Surface Processes and Landforms* **16**(1): 51–56.
McBride EF, Picard MD. 2004. Origin of honeycombs and related weathering forms in Oligocene Macigno Sandstone, Tuscan coast near Livorno, Italy. *Earth Surface Processes and Landforms* **29**(6): 713–735.
McGreevy JP. 1985. A preliminary scanning electron-microscope study of honeycomb weathering of sandstone in a coastal environment. *Earth Surface Processes and Landforms* **10**(5): 509–518.
Mellor A. 1986. A micromorphological examination of two Alpine soil chronosequences, Southern-Norway. *Geoderma* **39**(1): 41–57.
Mellor A, Short J, Kirkby SJ. 1997. Tafoni in the El Chorro area, Andalucia, southern Spain. *Earth Surface Processes and Landforms* **22**(9): 817–833.
Mottershead DN, Pye K. 1994. Tafoni on coastal slopes, south Devon, UK. *Earth Surface Processes and Landforms* **19**(6): 543–563.
Mustoe GE. 1982. The Origin of honeycomb weathering. *Geological Society of America Bulletin* **93**(2): 108–115.
Mustoe GE. 1983. Cavernous weathering in the Capitol Reef Desert, Utah. *Earth Surface Processes and Landforms* **8**(6): 517–526.
Norwick SA, Dexter LR. 2002. Rates of development of tafoni in the Moenkopi and Kaibab formations in Meteor Crater and on the Colorado Plateau, northeastern Arizona. *Earth Surface Processes and Landforms* **27**(1): 11–26.
Ollier CD. 1978. Inselbergs of the Namib Desert: processes and history. *Zeitschrift für Geomorphologie* (suppl. Bd. 31): 161–176.
Querol X, *et al*. 2000. Sources of natural and anthropogenic sulfur around the Teruel power station, NE Spain. Inferences from sulfur isotope geochemistry. *Atmospheric Environment* **34**(2): 333–345.
Rivas T, Prieto B, Silva B, Birginie JM. 2003. Weathering of granitic rocks by chlorides: effect of the nature of the solution on weathering morphology. *Earth Surface Processes and Landforms* **28**(4): 425–436.
Robinson DA, Williams RBG. 1987. Surface crusting of sandstone in southern England and northern France. In *International Geomorphology*, Gardiner V (ed). Wiley: 623–635.
Sancho C, Benito G. 1990. Factors controlling tafoni weathering in the Ebro basin (NE Spain). *Zeitschrift Fur Geomorphologie* **34**(2): 165–177.
Smith BJ. 1978. The origin and geomorphic implications of cliff foot recesses and tafoni on limestone hamadas in the northwestern Sahara. *Zeitschrift Fur Geomorphologie* (Neue Folge **23**): 21–43.
Stone JO. 2000. Air pressure and cosmogenic isotope production. *Journal of Geophysical Research – Solid Earth* **105**(B10): 23753–23759.
Sunamura T. 1996. A physical model for the rate of coastal tafoni development. *Journal of Geology* **104**(6): 741–748.
Tuckett F. 1884. Notes on Corsica. *Alpine Journal* **11**: 449–459.
Turkington AV, Phillips JD. 2004. Cavernous weathering, dynamical instability and self-organization. *Earth Surface Processes and Landforms* **29**(6): 665–675.
Twidale CBJ. 1976. The shaping and interpretation of large residual granite boulders. *Journal of Geological Society of Australia* **23**(4): 371–381.
Von Blanckenburg F, Hewawasam T, Kubik P. 2004. Cosmogenic nuclide evidence for low weathering and denudation in the wet, tropical highlands of Sri Lanka. *Journal of Geophysical Research* **109**. DOI: 10.1029/2003JF000049.
Wellman HW, Wilson AT. 1965. Salt weathering a neglected geological erosive agent in coastal and arid environments. *Nature* **205**(4976): 1097–1098.
White WM. 2005. *Geochemistry*. John Hopkins University Press.
Wilhelmy H. 1964. Cavernous rock surfaces (tafoni) in semiarid and arid climates. *Pakistan Geographical Review* **9**: 9–13.
Young ARM. 1987. Salt as an agent in the development of cavernous weathering. *Geology* **15**(10): 962–966.